THE JOURNAL OF NAVIGATION (2018), **71**, 1363–1380.
doi:10.1017/S0373463318000462

Improvement of Multi-GNSS Precise Point Positioning Performances with Real Meteorological Data

Ke Su[1,2] and Shuanggen Jin[1,3]

[1](*Shanghai Key Laboratory of Space Navigation and Positioning Technology, Shanghai Astronomical Observatory, Chinese Academy of Sciences, Shanghai 200030, China*)
[2](*University of Chinese Academy of Sciences, Beijing 100049, China*)
[3](*School of Remote Sensing and Geomatics Engineering, Nanjing University of Information Science and Technology, Nanjing 210044, China*)
(E-mail: sgjin@shao.ac.cn)

Tropospheric delay is one of the main error sources in Global Navigation Satellite System (GNSS) Precise Point Positioning (PPP). Zenith Hydrostatic Delay (ZHD) accounts for 90% of the total delay. This research focuses on the improvements of ZHD from tropospheric models and real meteorological data on the PPP solution. Multi-GNSS PPP experiments are conducted using the datasets collected at Multi-GNSS Experiments (MGEX) network stations. The results show that the positioning accuracy of different GNSS PPP solutions using the meteorological data for ZHD correction can achieve an accuracy level of several millimetres. The average convergence time of a PPP solution for the BeiDou System (BDS), the Global Positioning System (GPS), Global Navigation Satellite System of Russia (GLONASS), BDS+GPS, and BDS+GPS+GLONASS+Galileo are 55·89 min, 25·88 min, 33·30 min, 20·50 min and 15·71 min, respectively. The results also show that atmospheric parameters provided by real meteorological data have little effect on the horizontal components of positioning compared to the meteorological model, while in the vertical component, the positioning accuracy is improved by 90·6%, 33·0%, 22·2% and 19·8% compared with the standard atmospheric model, University of New Brunswick (UNB3m) model, Global Pressure and Temperature (GPT) model, and Global Pressure and Temperature-2 (GPT2) model and the convergence times are decreased 51·2%, 32·8%, 32·5%, and 32·3%, respectively.

KEYWORDS

1. GNSS. 2. PPP. 3. Tropospheric delay. 4. Meteorology.

Submitted: 29 November 2017. Accepted: 4 June 2018. First published online: 12 July 2018.

1. INTRODUCTION. Today, Global Navigation Satellite System (GNSS) Precise Point Positioning (PPP) uses available GNSS orbit and clock offset correction products to perform point positioning by a single GNSS receiver. The PPP technique requires a number

of accurate correction models to obtain a high-precision solution with undifferenced observations (Jin et al., 2004). Tropospheric delay is one of the most significant error sources in GNSS positioning, navigation and geodetic applications (Jin et al., 2009; 2010; 2011; Jin and Park, 2006). GNSS signals are affected by the Earth's atmosphere as they pass through the troposphere, causing a propagation delay of over two metres in the zenith direction (Jin et al., 2008). In precise positioning technology, the tropospheric delay is usually treated as Zenith Hydrostatic Delay (ZHD) and Zenith Wet Delay (ZWD) (Kouba, 2009); the latter is estimated directly as an unknown parameter, but the former is corrected by a non-meteorological model or a meteorological model in data processing. Atmospheric parameters such as pressure, temperature and water vapour pressure are needed for the meteorological model to calculate the Zenith Tropospheric Delay (ZTD) as in the Hopfield (1969) or Saastamoinen (1972) models, etc. Atmospheric parameters can be acquired from meteorological or some partial non-meteorological models at intervals of one day. Many GNSS stations are beginning to provide real observed meteorological data with a sampling rate of 30 s, which can explicitly show the variation of meteorological parameters and help study the impact of real measured atmospheric data on PPP.

Many scholars have assessed the performances of different tropospheric models. Leandro et al. (2006) concluded that the prediction errors of the University of New Brunswick (UNB3m) model have a mean bias of −0·5 cm and standard deviation of 4·9 cm based on ray-tracing analyses of 703,711 profiles from 223 stations in North America and surrounding territories from 1990 to 1996. Zhang et al. (2016) conducted a comprehensive study of the performances of a global three-dimensional grid-based ZTD model called IGGtrop, and European Geo-stationary Navigation Overlay System (EGNOS) and UNB3m models in China where the IGGtrop model performed the best. Hadas et al. (2013) applied various ZTD models to PPP using Bernese Global Positioning System (GPS) software and assessed the quality of the models. Ding et al. (2017) estimated the tropospheric delay and analysed the initialisation period and accuracy of the GNSS troposphere estimates. Yao et al. (2013) analysed the temporal-spatial variations of Global Zenith Troposphere Delay (GZTD) using the time series of Four-Dimensional (4D)-grid ZTD from 2002 to 2009 provided by the Global Geodetic Observing System (GGOS) compared to a series of University of New Brunswick (UNB) models.

There are numerous models that can calculate meteorological data including the standard atmospheric model, UNB3m model, Global Pressure and Temperature (GPT) model and Global Pressure and Temperature-2 (GPT2) model (Leandro et al., 2006; 2008; Böhm et al., 2007; Kouba, 2009; Lagler et al., 2013). Among them, the accuracy of the standard atmospheric model is the worst. Accordingly, this is also reflected in the PPP accuracy. The results of other meteorological models make little difference on PPP. Steigenberger et al. (2009) compared station coordinates with a global distribution obtained by different troposphere models, which showed that the site height differences computed with the GPT model and the European Centre for Medium-Range Weather Forecasts (ECMWF) numerical weather model data are below 1 mm in general, and the horizontal differences are even smaller. Real meteorological data can be obtained after daily observation collected by meteorological sensors and it can be applied for post-processing PPP. Precise hydrostatic delay calculated from meteorological data with high reliability and accuracy can improve the performance of PPP in satisfying the need for high precision navigation and positioning.

This paper addresses issues related to meteorological parameters and its influence on PPP. In Section 2, the different meteorological models including the standard atmospheric

model, UNB3m, GPT, and GPT2 are introduced. In Section 3, the multi-GNSS PPP processing strategy is proposed. In Section 4, experiments of different GNSS PPP with real meteorological data and the meteorological model to correct the ZHD are implemented to analyse the improvement of multi-GNSS PPP with real observed meteorological data. Finally, some conclusions and perspectives are given in Section 5.

2. METEOROLOGICAL MODELS.

2.1. *Standard atmospheric model.* The height-dependent values of pressure (P), temperature (T), and relative humidity (R_h) derived from a standard atmospheric model may be obtained by the equations:

$$P = P_0[1 - 0{\cdot}000226(H - H_0)]^{5{\cdot}225} \tag{1}$$

$$T = T_0 - 0{\cdot}0065(H - H_0) \tag{2}$$

$$R_h = R_{h0} \exp(-0{\cdot}0006396(H - H_0)) \tag{3}$$

where P_0, T_0 and R_{h0} are standard pressure, temperature and humidity at the reference height H_0 ($H_0 = 0$ m, $P_0 = 1013{\cdot}25$ mbar, $T_0 = 18^{\circ}$C, $R_{h0} = 50\%$) and H represents the height of the station.

The partial pressure of water vapor e (in mb) can be obtained by the equation:

$$e = R_h \exp(-37{\cdot}2465 + 0{\cdot}213166T - 0{\cdot}000256908T^2) \tag{4}$$

The meteorological parameters derived from the standard atmospheric model have low accuracy, which cannot reflect the temporal-spatial variations of atmospheric parameters (Kouba, 2009).

2.2. *UNB3m model.* Trenberth (1981) derived the UNB2 model based on the analysis of the Saastamoinen (1972) model considering the variation of the water vapour profile and latitude. With the latitude of the site according to the model, it is possible to calculate the average value of the meteorological parameters, including pressure, temperature, relative humidity, temperature lapse rate and water vapour pressure, but their temporal variation cannot be reflected (Swanson and Trenberth, 1981). Collins and Langley (1997) derived the UNB3 model using the standard meteorological datum to acquire the average value and yearly amplitude of five parameters. The user can obtain the value of meteorological parameters according to the latitude and epoch of the site to acquire the tropospheric delay. However, the part of the relative humidity converted from the water vapor pressure in the UNB3 model will exceed 100% (Collins and Langley, 1999). Hence, Leandro et al. (2008) refined the UNB3m model, which can calculate the relative humidity between 75% and 85%. In the UNB3m model, five output parameters including pressure, temperature, relative humidity, temperature lapse rate and water vapour pressure height factor can be acquired from the position of the site and the day of year. The meteorological parameter values for a particular latitude and day of the year can be obtained using a look-up

table (Leandro et al., 2008). The annual average and amplitude of given parameter can be computed as:

$$Avg_\phi = \begin{cases} Avg_{15}, \phi \le 15 \\ Avg_{75}, \phi \ge 75 \\ Avg_i + \dfrac{(Avg_{i+1} - Avg_i)}{15} \cdot (\phi - Lat_i), 15 < \phi < 75 \end{cases} \tag{5}$$

$$Amp_\phi = \begin{cases} Amp_{15}, \phi \le 15 \\ Amp_{75}, \phi \ge 75 \\ Amp_i + \dfrac{(Amp_{i+1} - Amp_i)}{15} \cdot (\phi - Lat_i), 15 < \phi < 75 \end{cases} \tag{6}$$

where ϕ is the latitude of the station of interest, Avg_ϕ is the computed average, Amp_ϕ stands for the computed amplitude, i is the index of the nearest lower tabled latitude and Lat represents latitude from the look-up table.

After the average and amplitude are computed at the given latitude, the parameter values P_0, T_0, RH_0, β_0 and λ_0 can be estimated in the desired day of year according to:

$$X_{\phi,doy} = Avg_\phi - Amp_\phi \cdot \cos\left[(doy - 28)\frac{2\pi}{365{\cdot}25}\right] \tag{7}$$

where $X_{\phi,doy}$ represents each computed parameter value for latitude ϕ and day of year doy. The conversion between relative humidity and water vapour pressure e_0 can be carried out as follows:

$$e_0 = \frac{RH_0}{100} \cdot e_s \cdot f_w \tag{8}$$

where the saturation vapour pressure e_s can be computed as:

$$\begin{aligned} e_s = {} & 0{\cdot}01 \cdot \exp(1{\cdot}2378847 \times 10^{-5} \times T_0^2) \\ & - 1{\cdot}912136 \times 10^{-2} \times T_0 + 33{\cdot}93711047 - 6{\cdot}3431645 \times 10^3 \times T_0^{-1}) \end{aligned} \tag{9}$$

The enhancement factor f_w can be determined as follows:

$$f_w = 1{\cdot}00062 + 3{\cdot}14 \times 10^{-6} \times P_0 + 5{\cdot}6 \times 10^{-7}(T_0 - 273{\cdot}15)^2 \tag{10}$$

Hence, the meteorological parameters can be represented as:

$$T = T_0 - \beta_0 * H \tag{11}$$

$$P = P_0 * \left(\frac{T}{T_0}\right)^{e_p} \tag{12}$$

$$e = e_0 * \left(\frac{T}{T_0}\right)^{e_p \lambda'} \tag{13}$$

where the power value of water vapour pressure $e_p = g/R/\beta_0$, g is the surface acceleration of gravity ($9{\cdot}80665\,\mathrm{ms}^{-2}$) (Tenzer et al., 2015), R is the gas constant for dry air ($287{\cdot}054\,\mathrm{J\,kg^{-1}\,K^{-1}}$), $\lambda' = 1 + \lambda$ and H is the orthometric height in m.

2.3. *GPT model.* In order to express the variation of the meteorological information in different places and times, Böhm et al. (2007) proposed the GPT model based on three years (September 1999 to August 2002) of 15° × 15° global grids of monthly mean profiles for pressure and temperature from ECMWF reanalysis data. The corresponding grid of orthometric heights of the Earth surface with respect to mean sea level is also available from the ECMWF. The parameters computed by the GPT model according to the station coordinate and day of the year can be expressed as:

$$\begin{bmatrix} P_0 \\ T_0 \end{bmatrix} = a_0 + A\cos\left(\frac{doy - 28}{365{\cdot}25} \times 2\pi\right) \tag{14}$$

where P_0 and T_0 are the mean value of pressure and temperature at mean sea level and doy is the day of year. The mean values a_0 and the annual amplitudes A expressed by degree and order nine are available:

$$a_0 = \sum_{n=0}^{9}\sum_{m=0}^{n} P_{nm}(\sin\varphi)\cdot[A_{nm}\cos(m\lambda) + B_{nm}\sin(m\lambda)] \tag{15}$$

where P_{nm} is the Legendre polynomials, φ and λ are latitude and longitude and A_{nm} and B_{nm} are the coefficients for degree n and order m. Hence, the meteorological parameter can be acquired by Equation (14).

2.4. *GPT2 model.* The GPT2 model is based on the global monthly mean profile of pressure, temperature, specific humidity and geopotential from ECMWF reanalysis of data from 2001 to 2010 (Lagler et al., 2013). It can provide the pressure P_0, temperature T_0, lapse rate dT and water vapour pressure e_0 at 5° × 5° grid intervals. With regard to the changing meteorological parameters, the mean values A_0, annual values (A_1, B_1) and semi-annual values (A_2, B_2) various calculations expressed by parameter $r(t)$ can be carried out as follows:

$$\begin{aligned} r(t) = A_0 &+ A_1\cos\left(\frac{doy}{365{\cdot}25}2\pi\right) + B_1\sin\left(\frac{doy}{365{\cdot}25}2\pi\right) \\ &+ A_2\cos\left(\frac{doy}{365{\cdot}25}4\pi\right) + B_2\sin\left(\frac{doy}{365{\cdot}25}4\pi\right) \end{aligned} \tag{16}$$

The inputs of the model are the coordinates of the site and epoch. The correction of the pressure P, temperature T and water vapour pressure e can be carried out as follows:

$$P = \frac{P_0 \times e^{-c\times H'}}{1000} \tag{17}$$

$$T = T_0 - dT \times H' \tag{18}$$

$$e = \frac{Q\cdot P}{0{\cdot}622} + 0{\cdot}378Q \tag{19}$$

where Q is the specific humidity, g_m is the gravity ($g_m = 9{\cdot}80665\,\mathrm{m/s^2}$), dM_r is the molar mass of dry air ($dM_r = 0{\cdot}0028965\,\mathrm{kg/mol}$) and R_g is the universal gas constant ($R_g = 8{\cdot}3143\,\mathrm{J/K/mol}$). H' is the orthometric height. The parameter c can be represented as:

$$c = \frac{g_m \times dM_r}{R_g \times T_0 \times (1 + 0{\cdot}6077 \times Q)} \tag{20}$$

3. PPP PROCESSING STRATEGY. The traditional model of PPP can be represented as (Zumberge et al., 1997):

$$P^s_{r,IF} = \frac{f_1^2 \cdot P_1 - f_2^2 \cdot P_2}{f_1^2 - f_2^2} = \rho^s_r + c(\delta t_r - \delta t^s) + T^s_r + e_{IF} \tag{21}$$

$$\Phi^s_{r,IF} = \frac{f_1^2 \cdot \Phi_1 - f_2^2 \cdot \Phi_2}{f_1^2 - f_2^2} = \rho^s_r + c(\delta t_r - \delta t^s) + T^s_r + \lambda_{IF} A_{IF} + \varepsilon_{IF} \tag{22}$$

where $P^s_{r,IF}$ is the Ionosphere-Free (IF) combination of pseudorange P_1 and P_2 observations at two distinct signal frequencies f_1 and f_2, $\Phi^s_{r,IF}$ is the IF combination of the corresponding carrier-phases Φ_1 and Φ_2 and ρ^s_r is the geometrical range from the satellite position at the signal emission epoch to the receiver position at its arrival epoch. δt_r is the receiver clock offset, δt^s is the satellite clock offset from the GNSS system time and c is the vacuum speed of light. T^s_r is the troposphere delay, A_{IF} is the non-integer ambiguity of the IF carrier phase combination, λ_{IF} is the IF combination of the carrier phase wavelengths and e_{IF} and ε_{IF} are the unmodelled multipath error and the relevant measurement noise components.

The observations are weighted with the satellite elevation angle. The stochastic model can be represented by a sinusoidal function (Witchayangkoon, 2000):

$$\sigma^2 = \frac{\sigma_0^2}{\sin^2(E)} \tag{23}$$

where E is the satellite elevation angle and σ_0 is the prior variance of the observations. When the observations of the pseusorange and carrier phase are used at the same time, the variance-covariance expression is:

$$\sigma^2 = \begin{bmatrix} \sigma_\rho^2 & 0 \\ 0 & \sigma_\phi^2 \end{bmatrix} \tag{24}$$

The experiment is carried out by using the multi-GNSS software developed independently. When the ionosphere effect is mitigated through the IF combination, the unknown parameters of the traditional PPP model are receiver position coordinates, receiver clock, ZHD and IF carrier phase ambiguities (non-integer). The GPS and GLONASS satellite Phase Centre Offset (PCO) and Phase Centre Variations (PCV) are corrected by the 'igs08_1861.atx' file generated by IGS. The BDS and Galileo antenna offset and variation recommended by Multi-GNSS Experiments (MGEX) are used to correct the PCO and PCV of BDS and Galileo satellites. The receiver PCO is derived from the components provided by the antenna file (Rizos et al., 2013). When integrated multi-GNSS PPP is carried out, additional system time difference is needed for each newly added GNSS system. The cut-off angle is set to 5°. A Kalman filter is used in the process of parameter estimation. The GPS and GLONASS code observation precision is set to 0·3 m and the phase observation precision is set to 0·003 m. The BDS and Galileo code observation precision is set to 0·6 m and the phase observation precision is set to 0·004 m (Cai et al., 2015). The values of parameters are determined by the precision of observations. The parameter estimation strategy in PPP is shown in Table 1. In data processing, the meteorological models listed in Section 2 and the real observed surface atmospheric parameters provided by the International GNSS Service (IGS) are used to provide the atmospheric parameters required for

Table 1. The parameter estimation strategy in PPP.

	Parameters	Ways
Observations	Pseudorange and carrier-phase	Undifferenced ionosphere-free linear combination PC and LC
	Cutoff elevations angular	5°
	Sampling rate	30s
Error model	Relativistic effects	IERS conventions 2010
	Earth rotation	IERS conventions 2010
	Solid Earth tides	IERS conventions 2010
	Ocean tides	IERS conventions 2010
	Earth pole tides	IERS conventions 2010
	Receiver antenna PCO and PCV	Model
	Satellite antenna PCO and PCV	Model
	Wind-up of satellite	Model
	Satellite clock bias	GBM product
	Satellite obit	GBM product
	Dry part of troposphere	Improved Hopfield model with mapping function
	Ionosphere	1st order effect eliminated by forming an ionosphere-free linear combination
Estimated parameters	Receiver coordinate	Estimation
	Wet part of troposphere	Estimation
	Receiver clock bias	Estimation
	Ambiguity	Estimation
	System time difference	Estimation

the improved Hopfield tropospheric model (Hopfield, 1969), to compute the ZHD, and to evaluate the impact on PPP. The ZWD is represented by a random-walk process and the receiver clock offset is estimated epoch-by-epoch. The power density of the tropospheric and receiver clock noise is set to $5\,\mathrm{mm\,hr^{-1/2}}$ and $100\,\mathrm{m\,s^{-1/2}}$, respectively (Hadas et al. 2017). The modified Hopfield model for calculating ZHD can be summarised as:

$$ZTD = ZD_{dry} + ZD_{wet}, ZD_i = 10^{-6} N_i \sum_{k=1}^{9} \frac{f_{k,i}}{k} r_i^k, i = dry, wet. \tag{25}$$

$$r_i = \sqrt{(R_E + h_i)^2 - R_E^2 \sin^2 z} - R_E \cos z \tag{26}$$

$$\begin{aligned} &f_{1,i} = 1, f_{2,i} = 4a_i, f_{3,i} = 6a_i^2 + 4b_i, f_{4,i} = 4a_i(a_i^2 + 3b_i), f_{5,i} = a_i^4 + 12a_i^2 b_i + 6b_i^2, \\ &f_{6,i} = 4a_i b_i(a_i^2 + 3b_i), f_{7,i} = b_i^2(6a_i^2 + 4b_i), f_{8,i} = 4a_i b_i^3, f_{9,i} = b_i^4 \end{aligned} \tag{27}$$

$$a_i = -\frac{\cos z}{h_i}, b_i = -\frac{\sin^2 z}{2h_i R_E} \tag{28}$$

$$h_d = 40,136 + 148{\cdot}72(T - 273{\cdot}15)(m), h_w = 11,000(m), \tag{29}$$

$$N_d = \frac{77{\cdot}64P}{T}(Kmb^{-1}), N_w = -\frac{12{\cdot}96e}{T} + \frac{371800e}{T^2}, R_E = 6378137m \tag{30}$$

where z is the zenith angle of the satellite, T is the temperature at the station (in units of Kelvin [K]), P is the atmospheric pressure (in units of millibars, mb), e is the partial pressure of water vapour (in mb), R_E is the Earth's radius, ZTD is the zenith tropospheric

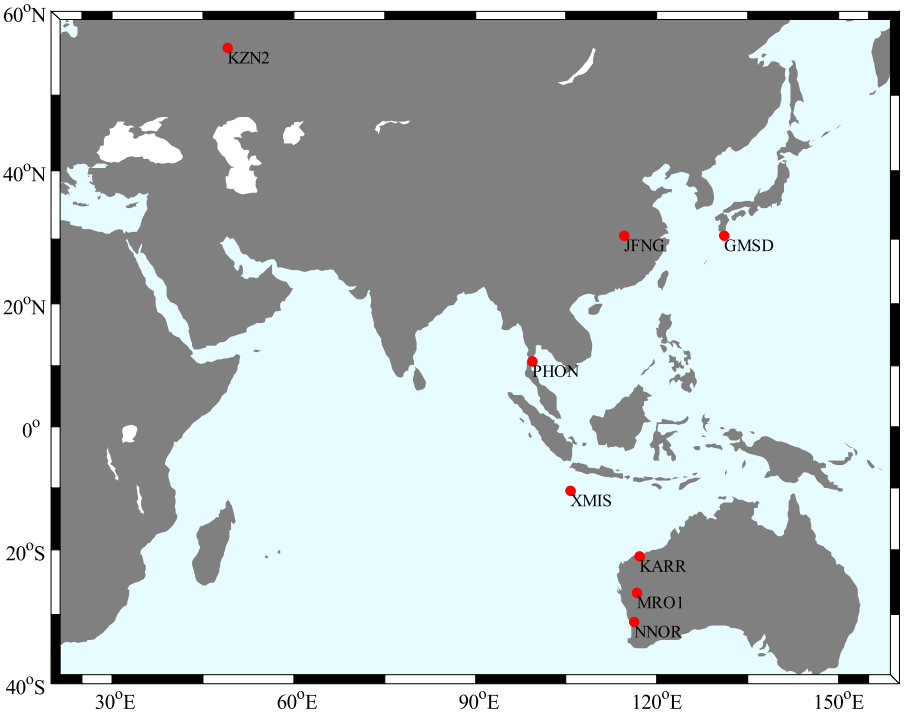

Figure 1. The distribution of the selected stations

delay, ZD_{dry} is the zenith tropospheric dry delay, ZD_{wet} is the zenith tropospheric wet delay, N is atmospheric refractivity for dry or wet component, r is the distance from the centre of the Earth to the station, h is the height and i represents dry or wet part of the delay. The convergence criterion is defined when the component of positioning coordinates is less than 0·1 m and keeping within 0·1 m in the subsequent 20 epochs. The positioning errors are calculated from the convergence epoch to the end epoch of a day.

4. RESULTS AND ANALYSIS.

4.1. *Data description.* The datasets were collected at eight IGS stations for the period of 1 to 15 May 2015 (day of year from 121 to 135). Figure 1 shows the distribution of the selected stations. All of the stations can receive quad-system observations from GPS, BDS, GLONASS and Galileo constellations. The processing strategy to obtain a PPP solution is listed in Table 1.

The observation data of XMIS station on 1 May 1 2015 was analysed as an example in the following subchapters. The XMIS station is located on Christmas Island, Australia. The type of antenna was JAVRINGANT_DM+ NONE. The data sampling rate of was 30 s. Figure 2 shows the partially observed satellite trajectory of BDS, GPS, GLONASS and Galileo on 1 May 1 2015. It shows that the satellite orbits of 13 BDS satellites (C01∼C14, except C13), 32 GPS satellites and 24 GLONASS satellites can be tracked. All BDS satellites, GPS satellites (G01∼G07), GLONASS satellites (R01∼R07) and Galileo satellites

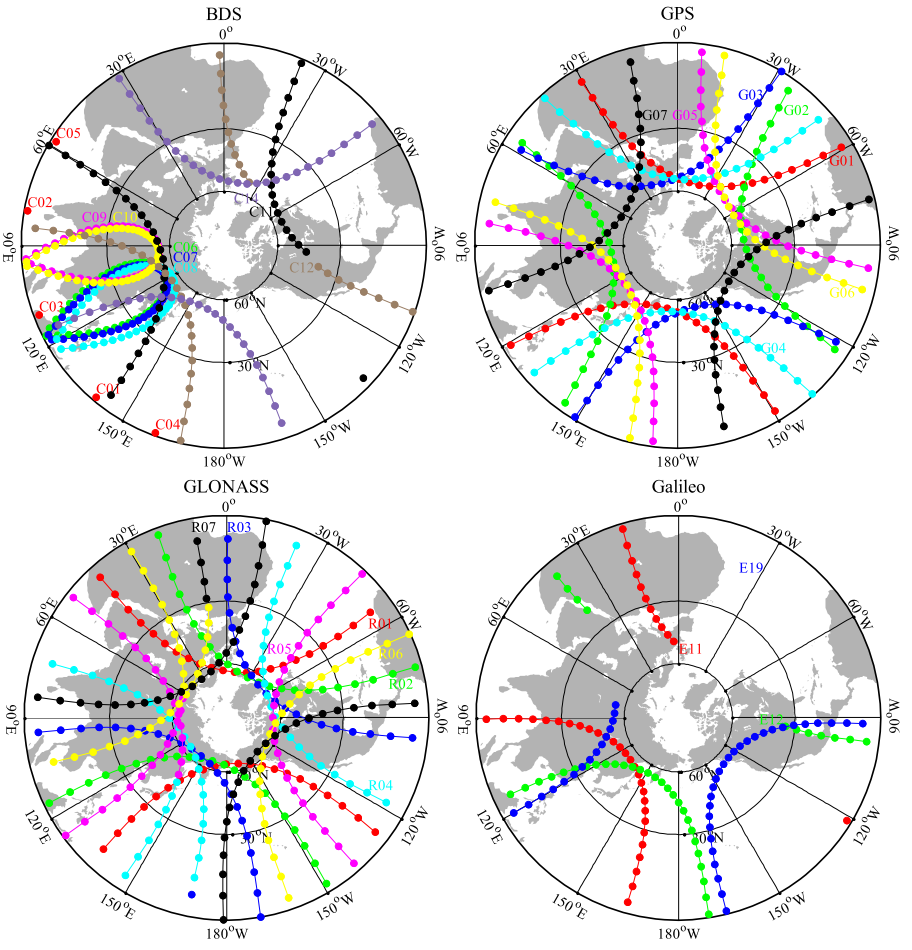

Figure 2. The partially observed satellite trajectory of BDS, GPS, GLONASS and Galileo at XMIS on 1 May 2015.

(E11, E12 and E19) are shown in the figure. The integration of different GNSS can significantly increase the number of visible satellites and obtain better zenith coverage. The BDS Geosynchronous Earth Orbit (GEO) satellites had the longest tracking periods, for example, C01∼C04 can be observed all day. The BDS Inclined Geosynchronous Orbit (IGSO) satellites C06∼C10 were tracked for a shorter period than GEO satellites, the Medium Earth Orbit (MEO) satellites were tracked for the shortest period. The number of visible satellites and the Position Dilution Of Precision (PDOP) of each combination (BDS, GPS, GLONASS, BDS+GPS, and four-system) at XMIS on 1 May 2015, are shown in Figure 3. At each epoch, The PDOP values for BDS, GPS and GLONASS are 0·5 ∼ 3, 1·5 ∼ 4 and 1 ∼ 6 respectively. The improvement of the spatial geometry is obvious under integrated multi-GNSS. It can be seen that the PDOP values in four-system PPP are below 1·0 in this period.

4.2. *Performance of different PPP solutions.* Figure 4 shows the results of different GNSS PPP solutions with real meteorological data-calculated ZHD at the XMIS station.

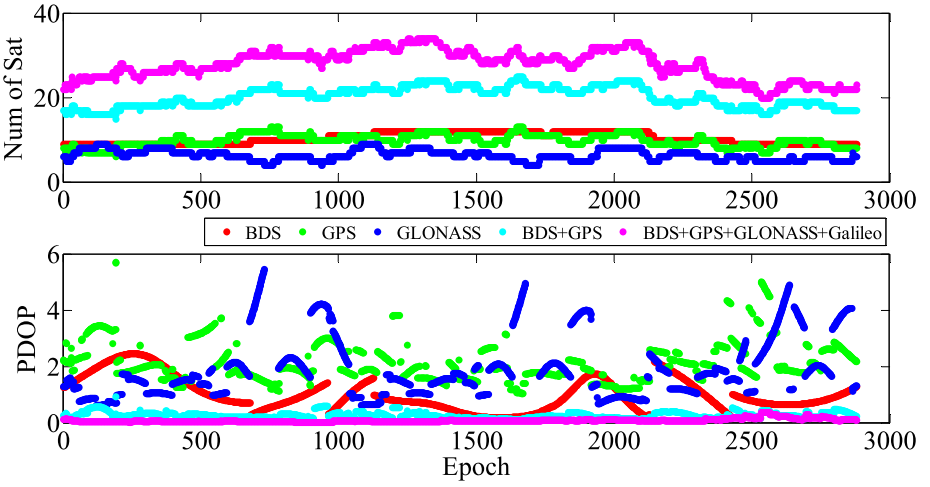

Figure 3. The number of visible satellites and PDOP of each combination (BDS, GPS, GLONASS, BDS+GPS, and four-system) at XMIS on 1 May 2015.

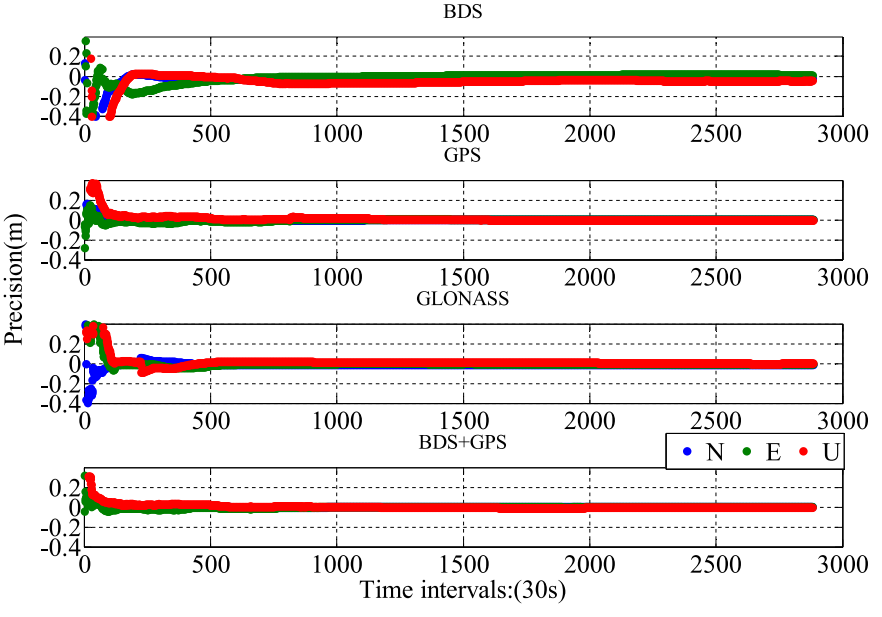

Figure 4. The result of BDS GPS, GLONASS and BDS+GPS PPP with real meteorological data at XMIS station.

At XMIS, the coordinate accuracy of BDS-only PPP was 5·7 mm, 12·9 mm and −14·6 mm in the north, east and up components while for GPS-only PPP the values were 2·9 mm, 4·3 mm and −5·6 mm, which is similar to BDS+GPS PPP, the position errors in three directions were 2·8 mm, 4·2 mm and −5·4 mm. For GLONASS-only PPP, the final positioning accuracy values were 4·3 mm, 5·5 mm and 9·1 mm. The positioning accuracy for different GNSS PPP can reach the level of several millimetres to centimetres. The statistical

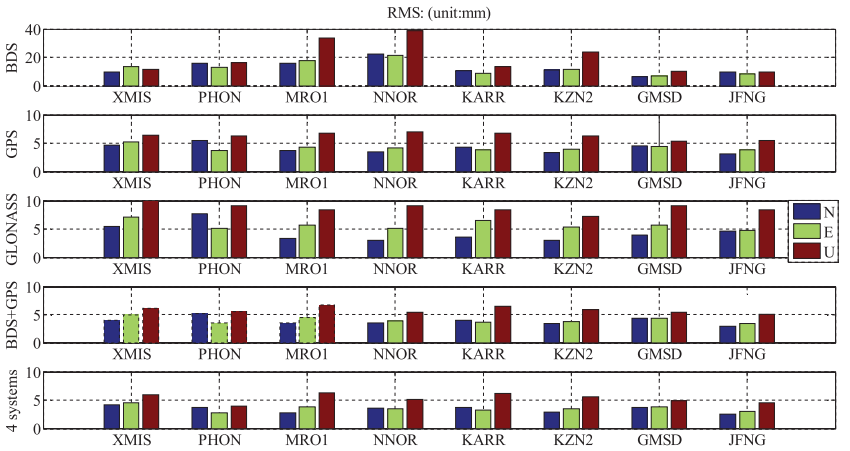

Figure 5. The average RMS in N, E and U coordinate of BDS PPP, GPS PPP, GLONASS PPP and BDS/GPS/GLONASS/Galileo PPP at the eight selected stations.

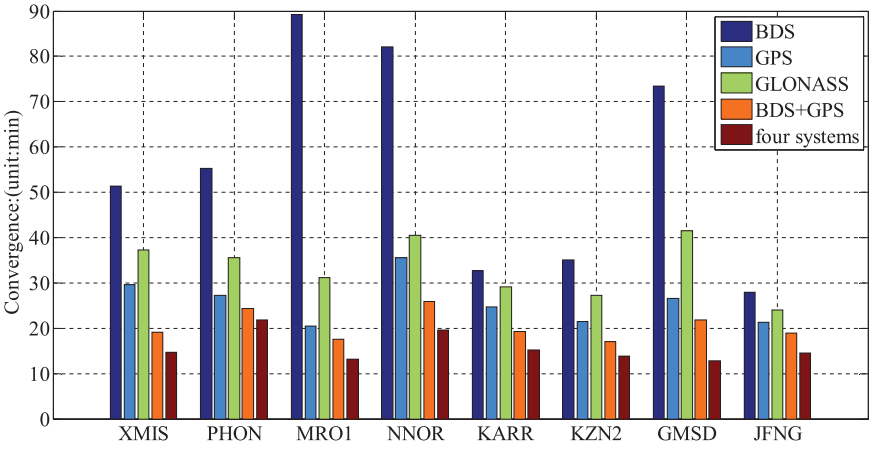

Figure 6. The average convergence time of BDS-only PPP, GPS-only PPP, GLONASS-only PPP and BDS+GPS+GLONASS+Galileo PPP at the eight selected stations.

convergence time of BDS-only, GPS-only, GLONASS-only and BDS+GPS was 53·0 min, 32·0 min, 36·5 min and 25·5 min, respectively.

In order to further evaluate the influence of the ZHD correction calculated by surface observed atmospheric parameters on BDS-only PPP, GPS-only PPP, GLONASS-only PPP and BDS+GPS+GLONASS+Galileo PPP, datasets collected at eight stations for 15 days were used. Figure 5 shows the average Root Mean Square (RMS) of position errors in the north, east and up components at the eight selected MGEX stations. Figure 6 gives the average convergence time of the corresponding stations.

According to Figures 5 and 6, we can draw the conclusion that the positioning accuracy of BDS-only PPP using surface observed meteorological data for ZHD corrections is the worst, which is mainly limited by the current distribution and number of BDS satellites and the orbit determination accuracy of the BDS constellation. Except for MRO1 and NNOR

Table 2. The meteorological parameters computed from four models in XMIS.

	Pressure (P: mbar)	Temperature (T: K)	Water vapor pressure (e: mbar)
Standard atmospheric model	736·9503	289·4597	7·9286
UNB3m model	983·3969	298·0020	23·3108
GPT model	978·4008	298·2460	23·8355
GPT2 model	979·8867	298·2460	26·2281

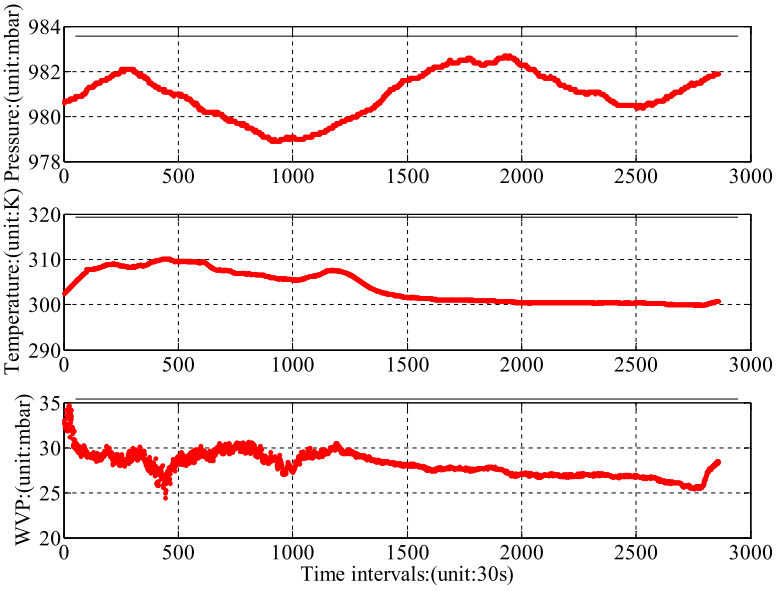

Figure 7. The variation of meteorological parameters provided by IGS on 1 May 2015.

stations, the RMS of position errors for BDS-only PPP in three directions is below 2·5 cm and the GPS-only PPP accuracy is slightly better than GLONASS-only PPP. The positioning accuracy of GPS-only PPP, BDS+GPS PPP, and BDS+GPS+GLONASS+Galileo PPP are approximately the same with observed meteorological data and the coordinate accuracy is better than 5 mm, 5 mm and 6 mm in the north, east and up components. Hence, integrated multi-GNSS PPP accuracy is not significantly improved in comparison with GPS-only PPP.

We can also conclude that the convergence time of BDS-only PPP is also the longest of the single systems and GPS-only is the best. Combination systems are obviously better than a single system. The average convergence time for different types of PPP is 55·89 min, 25·88 min, 33·30 min, 20·50 min and 15·71 min for BDS-only PPP, GPS-only PPP, GLONASS-only PPP and four systems PPP, respectively. Integrated quad-system PPP can significantly accelerate convergence, which is one of the toughest problems in current PPP solutions.

4.3. *Performance of PPP with different atmospheric parameters.* In order to evaluate the performance of improved Hopfield ZHD correction with surface observed

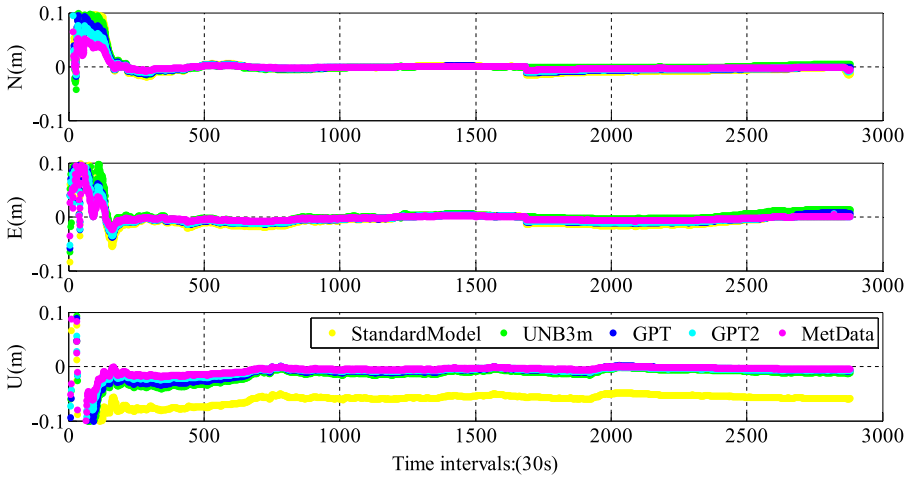

Figure 8. The results of BDS+GPS+GLONASS+Galileo PPP utilising different meteorological models and real data.

Table 3. The RMS value of multi-PPP by different methods.

	StandardModel(mm)			UNB3m(mm)			GPT(mm)			GPT2(mm)			MetData(mm)		
Stations	N	E	U	N	E	U	N	E	U	N	E	U	N	E	U
XMIS	5·1	6·1	60·8	4·8	5·5	8·9	4·6	5·3	8·1	4·5	5·1	7·4	4·1	4·5	6·0
PHON	5·9	4·0	54·0	5·9	3·8	5·9	5·9	3·9	5·0	5·4	3·5	5·1	3·6	2·8	3·9
MRO1	4·5	5·3	56·8	3·8	4·9	8·3	3·5	4·6	7·3	3·0	4·4	7·4	2·8	3·9	6·4
NNOR	6·0	5·4	54·1	5·6	5·1	8·0	5·1	4·5	7·3	5·1	4·0	7·0	3·6	3·5	5·1
KARR	4·9	5·6	62·1	4·4	3·8	8·1	4·3	3·5	7·6	4·1	3·5	7·4	3·6	3·2	6·1
KZN2	3·8	4·3	57·4	3·4	4·1	8·4	3·0	3·9	7·1	2·9	3·9	6·8	2·9	3·5	5·6
GMSD	4·5	4·9	52·5	4·3	4·5	6·9	4·3	4·3	6·3	4·0	4·1	6·0	3·6	3·9	4·9
JFNG	3·3	4·3	54·8	3·0	3·8	8·9	2·8	3·4	5·9	2·8	3·4	5·9	2·5	3·0	4·5
RMS	4·8	5·0	56·6	4·4	4·5	7·9	4·1	4·1	6·8	3·9	4·0	6·6	3·3	3·5	5·3

meteorological data in GNSS PPP, the results of BDS+GPS+GLONASS+Galileo quad-system PPP are compared with the atmospheric parameters provided by the standard atmospheric model, UNB3m, GPT and GPT2 for ZHD correction in PPP. The meteorological parameters computed from four models at the XMIS station on 1 May 2015 are listed in Table 2, and Figure 7 gives the time series of surface observed meteorological parameters provided by IGS, whose sampling rate is 30 s.

From Table 2, it can be seen that the atmospheric parameters derived from meteorological models are the daily average. Hence, the model outputs cannot reflect the sub-diurnal variation characteristics of atmospheric parameters. There are also significant deviations between the standard atmospheric model and the other models. Taking the surface measured data as the reference, the accuracy of water vapour pressure provided by GPT2 is slightly better than that from UNB3m and GPT. The performances of integrated multi-PPP are examined and the meteorological parameters needed in the improved Hopfield model for ZHD correction provided by observed data and meteorological models are evaluated in a PPP solution. Other model corrections for PPP are listed in Table 1. Figure 8 shows

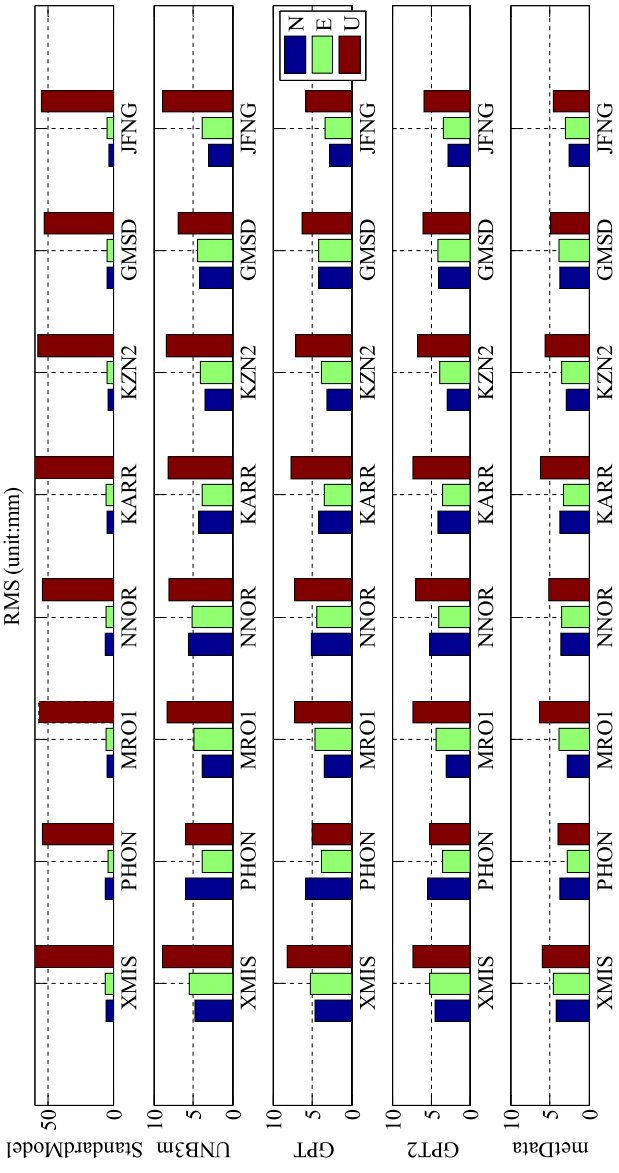

Figure 9. RMS value of multi-PPP in three-dimensions of different station by different methods.

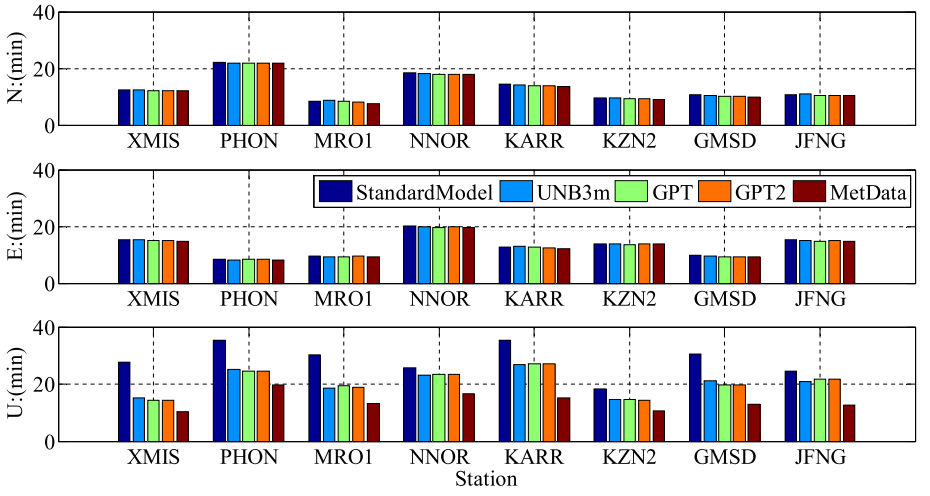

Figure 10. The average convergence time at the selected eight stations with different atmospheric parameter sources for ZHD correction.

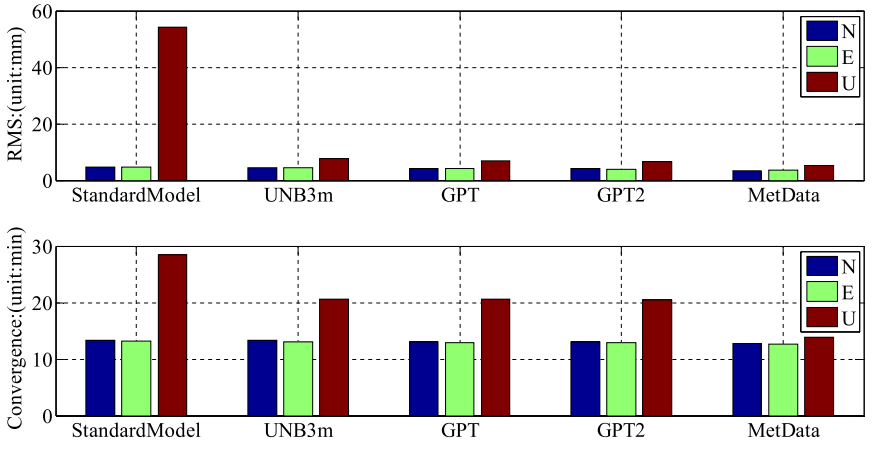

Figure 11. The average convergence time of multi-PPP in three components with different atmospheric parameter sources for ZHD correction.

the position error series of BDS+GPS+GLONASS+Galileo PPP in the north, east and up components. Where StandardModel stands for the results using the standard atmospheric model, UNB3m represents that the UNB3m model is adopted, GPT stands for the PPP strategy with GPT model outputs for ZHD correction and GPT2 and MetData stand for the results using the GPT2 model and observed meteorological data.

The positioning results of the BDS+GPS+GLONASS+Galileo PPP with ZHD correction using the atmospheric parameters provided by real meteorological data and the output values from the standard atmospheric model, UNB3m, GPT and GPT2 are analysed. Table 3 and Figure 9 show the RMS values of position errors in the north, east and up

components at eight stations. Figure 10 shows the average convergence time in three directions at corresponding stations. Figure 11 gives the statistical results of position accuracy and convergence time with different atmospheric parameter sources for ZHD correction.

By comparing Table 3, Figure 9 and Figure 11, it can be seen that the RMS of positioning error in the up component is obviously bigger than that in the north and east components. When the atmospheric parameters provided by the standard atmospheric model for computing ZHD corrections in muti-GNSS PPP is used, the RMS of positioning error in the up component is ten times bigger than the horizontal components. The result of PPP using real atmospheric data is the best and the RMS of position error for the other three models is almost the same. The statistical coordinate differences in the north and east components for all of the atmospheric parameter sources are lower than 1·4 mm. Hence, the ZHD model with accurate atmospheric parameters benefits the position accuracy in the up component. Compared with the observed meteorological parameters, the RMS of position error with the model parameters from the standard atmospheric model, UNB3m, GPT, and GPT2 can be decreased by 90·6%, 33·0%, 22·2% and 19·8%, respectively. The convergence time of integrated multi-GNSS PPP in the horizontal directions are almost the same, as shown in Figures 10 and 11. The convergence time for the four meteorological models in the up component is 28·48 min, 20·68 min, 20·59 min and 20·53 min, respectively. It only takes 13·90 min for surface observed atmospheric parameters to converge and the convergence efficiency is improved by 51·2%, 32·8%, 32·5% and 32·3%, respectively.

5. CONCLUSION. The aim of this paper is to study the performance of PPP using real meteorological data for ZHD correction. Firstly, this contribution summarises the standard atmospheric model, UNB3m, GPT and GPT2 meteorological models, which are usually adopted for providing atmospheric parameters for calculating the ZHD correction. Then the multi-GNSS PPP experiments are carried out to evaluate the impact of ZHD correction with different sources of atmospheric parameters on the positioning solution.

The accuracy of different GNSS PPP solutions using real atmospheric parameters for ZHD correction can reach several millimetres. The statistical results show that the BDS-only PPP accuracy is the worst for a single GNSS system, the average RMS of positioning errors is 13·6 mm, 13·5 mm and 20·5 mm in the north, east and up components while the ones for GPS-only PPP are the best. BDS+GPS PPP and BDS+GPS+GLONASS+Galileo PPP can slightly improve the positioning accuracy, and the RMS of positioning errors in three directions is lower than 5 mm, 5 mm and 6 mm. According to our convergence criterion, the average convergence time for BDS-only PPP, GPS-only PPP, GLONASS-only PPP, BDS+GPS PPP and BDS+GPS+GLONASS+Galileo PPP is 55·89 min, 25·88 min, 33·30 min, 20·50 min and 15·71 min, respectively; integrated multi-GNSS PPP significantly contributes to improving the convergence time, which is of high value in improving the utility of PPP.

Compared with atmospheric parameters provided by meteorological models for ZHD correction computing in PPP, the improvement of positioning accuracy with real atmospheric data is not obvious in horizontal components. As we know that there is a strong link between the coordinate solution in the up component and tropospheric delay, our experimental results confirm that using externally observed meteorological parameters for troposphere hydrostatic correction in PPP can greatly benefit the accuracy of coordinates in the up component, compared to the parameters provided by the standard atmospheric

model, UNB3m, GPT and GPT2 computing ZHD for a PPP solution. The vertical RMS of positioning errors can be improved by 90·6%, 33·0%, 22·2% and 19·8% respectively. The convergence time in the up component is decreased by 51·2%, 32·8%, 32·5% and 32·3%, respectively.

ACKNOWLEDGEMENTS

This research is supported by the National Natural Science Foundation of China (NSFC) Project (Grant No. 11573052). The authors gratefully acknowledged the GFZ for providing products and IGS for the data from MGEX.

REFERENCES

Böhm, J., Heinkelmann, R. and Schuh, H. (2007). Short note: a global model of pressure and temperature for geodetic applications. *Journal of Geodesy*, **81**(10), 679–683.

Cai, C., Gao, Y., Pan, L. and Zhu, J. (2015). Precise point positioning with quad-constellations: GPS, BeiDou, GLONASS and Galileo. *Advances in Space Research*, **56**(1), 133–143.

Collins, J. P. and Langley, R. B. (1997). *A tropospheric delay model for the user of the wide area augmentation system*. Department of Geodesy and Geomatics Engineering, University of New Brunswick.

Collins, J. P. and Langley, R. B. (1999). *Nominal and extreme error performance of the UNB3 tropospheric delay model*. Department of Geodesy and Geomatics Engineering, University of New Brunswick, 173pp.

Ding, W., Teferle, F. N., Kazmierski, K., Laurichesse, D. and Yuan, Y. (2017). An evaluation of real-time troposphere estimation based on GNSS Precise Point Positioning. *Journal of Geophysical Research: Atmospheres,* **122**(5), 2779–2790.

Hadas, T., Kaplon, J., Bosy, J., Sierny, J. and Wilgan, K. (2013). Near-real-time regional troposphere models for the GNSS precise point positioning technique. *Measurement Science and Technology*, **24**(5), 055003.

Hadas, T., Teferle, F. N., Kazmierski, K., Hordyniec, P. and Bosy, J. (2017). Optimum stochastic modeling for GNSS tropospheric delay estimation in real-time. *GPS Solutions*, **21**(3), 1069–1081.

Hopfield, H.S. (1969). Two-quartic tropospheric refractivity profile for correcting satellite data. *Journal of Geophysical Research*, **74**(18), 4487–4499.

Jin, S.G., Han, L. and Cho, J. (2011). Lower atmospheric anomalies following the 2008 Wenchuan Earthquake observed by GPS measurements. *Journal of Atmospheric and Solar-Terrestrial Physics*, **73**(7–8), 810–814, doi: 10.1016/j.jastp.2011.01.023.

Jin, S.G., Li, Z.C. and Cho, J.H. (2008). Integrated water vapor field and multi-scale variations over China from GPS measurements. *Journal of Applied Meteorology and Climatology*, **47**(11), 3008–3015, doi: 10.1175/2008JAMC1920.1.

Jin, S.G., Luo, O.F. and Gleason, S. (2009). Characterization of diurnal cycles in ZTD from a decade of global GPS observations. *Journal of Geodesy*, **83**(6), 537–545, doi: 10.1007/s00190-008-0264-3.

Jin, S.G., Luo, O.F. and Ren, C. (2010). Effects of physical correlations on long-distance GPS positioning and zenith tropospheric delay estimates. *Advances in Space Research*, **46**(2), 190–195, doi: 10.1016/j.asr.2010.01.017.

Jin, S.G., and Park, P.H. (2006). Strain accumulation in South Korea inferred from GPS measurements. *Earth, Planets and Space*, **58**(5), 529–534, doi: 10.1186/BF03351950.

Jin, S.G., Wang, J., Zhang, H. and Zhu, W.Y. (2004). Real-time monitoring and prediction of the total ionospheric electron content by means of GPS observations, *Chinese Astronomy and Astrophysics*, **28**(3), 331–337, doi: 10.1016/j.chinastron.2004.07.008.

Kouba, J. (2009). Testing of global pressure/temperature (GPT) model and global mapping function (GMF) in GPS analyses. *Journal of Geodesy*, **83**(3), 199–208.

Lagler, K., Schindelegger, M., Böhm, J., Krásná, H. and Nilsson, T. (2013). GPT2: Empirical slant delay model for radio space geodetic techniques. *Geophysical research letters*, **40**(6), 1069–1073.

Leandro, R., Santos, M. C. and Langley, R. B. (2006). UNB neutral atmosphere models: development and performance. *In Proceedings of ION NTM*. 2006, **52**(1), 564–73.

Leandro, R. F., Langley, R. B. and Santos, M. C. (2008). UNB3m_pack: a neutral atmosphere delay package for radiometric space techniques. *GPS Solutions*, **12**(1), 65–70.

Rizos, C., Montenbruck, O., Weber, R., Weber, G., Neilan, R. and Hugentobler, U. (2013). The IGS MGEX experiment as a milestone for a comprehensive multi-GNSS service. In: *Proceedings of the ION 2013 Pacific PNT Meeting (ION-PNT-2013), April 23–25, Honolulu, Hawaii, USA*, 289–295.

Saastamoinen, J. (1972). Atmospheric correction for the troposphere and stratosphere in radio ranging satellites. *Use of Artificial Satellites for Geodesy*, **15**(6), 247–251.

Steigenberger, P., Boehm, J. and Tesmer, V. (2009). Comparison of GMF/GPT with VMF1/ECMWF and implications for atmospheric loading. *Journal of Geodesy*, **83**(10), 943–951.

Swanson, G. S. and Trenberth, K. E. (1981). Trends in the Southern Hemisphere tropospheric circulation. *Monthly Weather Review*, **109**(9), 1879–1889.

Tenzer, R., Chen, W., Tsoulis, D., Bagherbandi, M., Sjoberg, L., Novak, P. and Jin S.G. (2015). Analysis of the refined CRUST1.0 crustal model and its gravity field. *Survey Geophysics*, **36**(1), 139–165, doi: 10.1007/s10712-014-9299-6.

Trenberth, K. E. (1981). Seasonal variations in global sea level pressure and the total mass of the atmosphere. *Journal of Geophysical Research: Oceans*, **86**(C6), 5238–5246.

Witchayangkoon, B. (2000). *Elements of GPS Precise Point Positioning*. Ph.D. dissertation, Department of Spatial Information Science and Engineering, University of Maine, Orono, Maine, U.S.A.

Yao, Y., He, C., Zhang, B. and Xu, C. (2013). A new global zenith tropospheric delay model GZTD. *Chinese Journal of Geophysics-Chinese Edition*, **56**(7), 2218–2227.

Zhang, H., Yuan, Y., Li, W., Li, Y. and Chai, Y. (2016). Assessment of three tropospheric delay models (IGGTROP, EGNOS and UNB3M) based on precise point positioning in the Chinese region. *Sensors*, **16**(1), 122.

Zumberge, J. F., Heflin, M. B., Jefferson, D. C., Watkins, M. M. and Webb, F. H. (1997). Precise point positioning for the efficient and robust analysis of GPS data from large networks. *Journal of Geophysical Research: Solid Earth*, **102**(B3), 5005–5017.